Journal of Alloys and Compounds 728 (2017) 1–9

Contents lists available at ScienceDirect

Journal of Alloys and Compounds

journal homepage: http://www.elsevier.com/locate/jalcom

Scalable preparation of mesoporous Silicon@C/graphite hybrid as stable anodes for lithium-ion batteries

Xiaotian Li [a], Dandan Yang [a], Xiaocun Hou [a], Jinhong Shi [a], Yi Peng [a], Huabin Yang [a, b, *]

[a] Institute of New Energy Material Chemistry, School of Materials Science and Engineering, Nankai University, Tianjin 300350, China
[b] Tianjin Key Laboratory of Metal and Molecule Based Material Chemistry, China

ARTICLE INFO

Article history:
Received 23 November 2016
Received in revised form
23 August 2017
Accepted 27 August 2017
Available online 30 August 2017

Keywords:
Mesoporous Si@C/graphite composite
Acid etching process
Al-Si alloy
Anode material
Lithium ion batteries

ABSTRACT

A mesoporous Si@amorphous carbon/graphite (Si@C/G) material is synthesized by acid etching technique on a low-cost Al-Si alloy followed by ball-milling and heat treatment process. The Galvanostatic charge/discharge tests prove that the specific anodes hold a high gravimetric capacity of 919.0 mAh g^{-1} after 150 cycles. In addition, benefiting from the addition of the graphite, a relatively high initial coulombic efficiency of 78.4% is achieved. The physical-chemical properties are characterized by SEM, XRD, XPS, TEM and N_2 sorption methods, revealing that the mesoporous Si is coated by amorphous carbon layer, ca. 20 nm. The mesoporous structure of Si can refrain the volume expansion of hybrid material during the lithium insertion/extraction process and can create efficient channels for the fast transport of Li^+, and the outer carbon layer and graphite can increase the electroconductibility of the anode material. This low-cost Si@C/G hybrid material with improved electrochemical properties via a simple and applicable synthesis process on Al-Si alloy is prospective for scalable production in commercial lithium ion batteries.

1. Introduction

Considering the soaring progress of mobile electronic equipment, the market need of rechargeable lithium ion batteries with high specific capacity, long lifespan and superior rate capability is increasing obviously [1]. However, the commercial graphite anode is hindered for further application in high-performance lithium-ion batteries due to its low theoretical gravimetric capacity (372 mAh g^{-1}) [2]. Silicon is regarded as one of the best substitutes for graphite on account of its high theoretical specific capacity of about 4200 mAh g^{-1} when alloyed with Li as the form of $Li_{4.4}Si$ and low working voltage of 0.5 V (vs. Li/Li^+) [3–6]. However, the rapid decrease of specific capacity caused by the low electric conductivity and the severe volume expansion (>300%) during Li insertion/extraction process hinder its commercial application [7–9].

Great efforts have been done to overcome these shortcomings of Si through decreasing Si particle size [10–12], fabricating silicon-based films [13,14], compositing with active/inactive matrix and forming specific structure [15–17]. Recent work has demonstrated that the combination of Si and C can take both advantages of high lithium storage capacity and long lifespan to improve the overall properties of the silicon anodes [18–24]. Diverse structural Si/C composites were synthesized through different approaches, including Si/graphene composites via graphenic scaffold with in-plane carbon vacancy defects [25], mesoporous Si/C composites via magnesium-thermal reduction process [16,26–28], Si@void@C composites via the removal of SiO_2 [29,30], Si/C nanoparticles via CVD process [31], and C/Si/C trilayer nanomembranes via rolled-up nanotechnology [32]. The electrochemical properties of the above materials are superior due to the cyclic stability and relative high specific capacity. Nevertheless, the high cost of manufacture and the difficulty in large-scale production impeded the commercial application. To solve these problems, lots of researchers devoted themselves to seeking for cheap Si source and industrially feasible methods. It was reported that the porous Si can be fabricated through electrochemical etching [33] or acid etching [34–36]. Micro-sized nano-porous Si/C anodes were obtained through an acid etching on Al-Si alloy and ball milling process by Tian and his coworkers [35]. It represented a 86.8% capacity retention, ca.1182 mAh g^{-1} after 300 cycles, at the current density of 50 mA g^{-1}. However, the high specific surface area incurred the

* Corresponding author. Institute of New Energy Material Chemistry, School of Materials Science and Engineering, Nankai University, Tianjin 300350, China.
E-mail address: hb_yang@nankai.edu.cn (H. Yang).

http://dx.doi.org/10.1016/j.jallcom.2017.08.244
0925-8388/

decreased energy density of the Li-ion batteries, and the initial coulombic efficiency was only ca. 60%, which significantly hindered the mass-scaled industrial production, eventually. Over the last several years, many mesoporous Si/C materials are reported for Li ion battery. But most of the mesoporous Si materials are synthesized by template and high-temperature reduction methods, which are high cost, time-consuming and environment-unfriendly.

For handling the defect of low initial coulombic efficiency (ICE) and reducing the cost of raw materials of the porous Si/C composites, a carbon-coated mesoporous Si particle dispersing in graphite is prepared by an acid etching on a low-cost Al-Si alloy after a high energy mechanical milling (HEMM) and heat treatment procedure in this work. Herein, commercially available Al-Si alloy powder, graphite and sucrose were used as raw materials. The existence of the mesopores in the as-prepared Si@C/G material could buffer the volume expansion obviously, which led to a preferable electrochemical performance than pristine Si@C/G [37]. The enhancement of the electric conductivity caused by the addition of the graphite generated a higher initial coulombic efficiency (78.4%) compared with the previous report (61%) [35].

2. Experimental

2.1. Material synthesis

The commercial Al-Si alloy powder (75% Al, 25% Si) was obtained from Hunan Ningxiang Jiweixin Metal Powder Co. Ltd., China. Graphite and sucrose were gained from Tianjin Chemical Co. Ltd., China. All chemicals were put to use as received.

2.1.1. The preparation of porous Si dispersed in graphite

2 g Al-Si alloy power and graphite were milled for 4 h by a HEMM technique with a rotational velocity of 400 rpm. Afterwards, the compound was etched by an excess dilute HCl solution (1 mol L^{-1}) for 12 h. Then suction filtration and washing with deionized water and ethanol were conducted to get a neutral solution. The mixture was stoved in a vacuum oven at 80 °C for 24 h to get the composite as standby.

2.1.2. The synthesis of mesoporous Si@C/G material

The above prepared composite was mixed with sucrose in a weight proportion of 3:5 via HEMM for 4 h. Afterwards, the mixture was pyrolyzed at 800 °C for 4 h to obtain a structure of silicon coated by amorphous carbon. Finally, the ultimate mesoporous material was constitutive of the Si@C composite and the graphite with a theoretical mass ratio of 1:1.

A prinstine Si@C/G material whose Si source was micro-sized was prepared by a similar HEMM and pyrolysis process as a comparison. Typically, the micro-sized Si and graphite were milled for 4 h by a HEMM technique with a rotational velocity of 400 rpm in a weight proportion of 1:2. Then the Si/G composite was mixed with sucrose in a weight proportion of 3:5 via HEMM for 4 h. Afterwards, the mixture was pyrolyzed at 800 °C for 4 h to obtain a structure of silicon coated by amorphous carbon. All the ratio of ball-to-powder weight was 10:1.

2.2. Structural characterization

The crystallinity of the anode material was characterized by X-ray diffraction (XRD) measurement on Rigaku D/max-2500 X-ray diffractometer with Cu-Kα radiation. The specific surface area and the pore size distribution were measured by a Quantachrome NOVA 2000e sorption analyzer at 77 K. The morphology, elemental mapping images, elementary composition and microstructures of the powders were characterized by a scanning electron microscopy (SEM, JEOL JSM-7500F), an electron dispersive spectrometer (EDS) and a transmission electronic microscopy (TEM, FEI Tecnai G2 F20). Thermogravimetric (TG) curve was obtained on a TG209 apparatus (NETZSCH Company, Germany) with a ramping speed of 10 °C min^{-1} under air atmosphere.

2.3. Electrochemical measurement

The active material, carbon black and polyvinylidene fluoride (PVdF) (80:10:10 in mass) were mingled in the N-methylpyrrolidinone (NMP) for 24 h to obtain a homogeneous slurry. Afterwards, we deposited it onto the surface of the Cu foil. Finally, the slice was dried at 120 °C for 15 h under vacuum. After a series of treatments, we got the appropriate size of disk as working electrodes of coin-type cells (CR2032), which were assembled with the Celgard 2400 as the separator and lithium wafers as the counter electrodes. The electrolyte was constituted of 1 M $LiPF_6$ as the solute, as well as the ethylene carbonate (EC) and dimethyl carbonate (DMC) (1:1 in volume ratio) as the solvent.

A Solartron 1287 comprehensive electrochemical power workstation was employed to measure the cyclic voltammetry (CV) curves with a voltage range of 0–3.0 V at a sweeping rate of 0.1 mV s^{-1}. Electrochemical impedance spectroscopic (EIS) test was performed with an alternating current amplitude of 5 mV in the frequency of 10^{-2} Hz to 10^{5} Hz by a Solartron 1250 impedance measure analyzer coupled with a Solartron 1287 Electrochemical Interface. The constant current charge and discharge tests were performed at a current density of 100 mA g^{-1} along with the cut-off voltage of 0.01–3.0 V versus Li/Li^{+}. All the measurements were conducted at 25 °C.

3. Results and discussion

3.1. Structure and morphology characterizations

The XRD patterns of the Al-Si alloy, the Al-Si alloy after etching and the mesoporous Si@C/G are given in Fig. 1. The strong diffraction peaks of Si (2θ = 28.4°, 47.3°, 56.1°, 69.1°, 76.4°) and Al (2θ = 38.5°, 44.7°, 65.1°, 78.2°) can be distinctly observed before the acid etching, implying that the Si and Al phases in the original material exist separately without forming any new alloy phase. As the Al-Si mixture is one type eutectic, we still denote it as a kind of

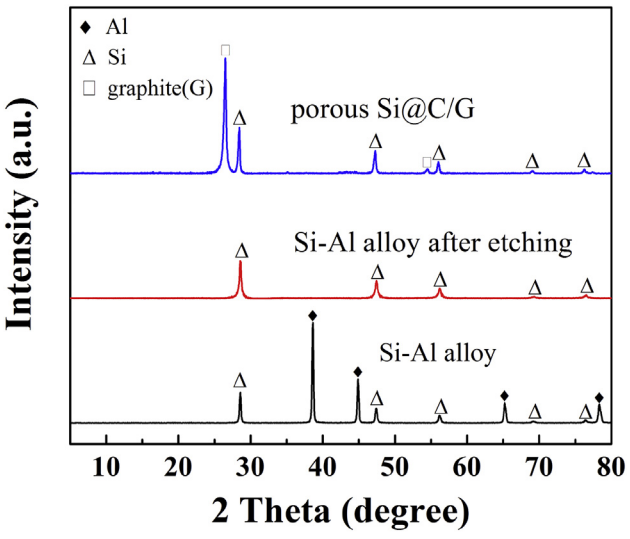

Fig. 1. XRD patterns of the Al-Si and the mesoporous Si@C/G composite.

alloy, which is in accordance with the previous report [36]. The Al patterns disappear entirely after the acid etching process, which is in keeping with the XPS survey scan of the mesoporous Si@C/G provided in Fig. S1, avoiding forming nucleation potential [38] and emerging poor circulation performance. The diffraction peaks indexed to Si and graphite ($2\theta = 26.5°, 54.7°$) in the XRD patterns of mesoporous Si@C/G can be clearly observed. Meanwhile, The Si 2p XPS spectrum of the mesoporous Si@C/G given in Fig. S2 and the relative content (wt%) of Si^0 and Si^{4+} showed in Table S1 reveal that the content of the Si^0 (sputtering 5min) is more than that of without sputtering, indicating the existence of the SiO_2 layer at the surface [39]. However, due to the low crystallization of the amorphous carbon, its diffraction peaks are overlapped by the graphite which is coincided with the previous reports [39–41]. The existence of the graphite can enhance the electric conductivity of the material, which is much favourable for the cycling stability of lithium ion batteries anodes.

The N_2 sorption analysis (Fig. 2) is applied to assess the textural property. The N_2 adsorption-desorption isotherms of the porous Si are close to Type IV with a large specific surface area of 292 $m^2\ g^{-1}$, which can be attributed to the capillary condensation in a mesopores structure [42,43]. After the ball milling and pyrolysis, the isotherms of the Si@C/G change to type III. And the corresponding specific surface area calculated by the Brunauer–Emmett–Teller (BET) method decreases to 118 $m^2\ g^{-1}$. Nevertheless, it is still much larger than that in the literature (37 $m^2\ g^{-1}$) [35]. Correspondingly, the pores distribute around 3–8 nm both in the two materials calculated by Non-Local-DFT, suggesting that the Si@C/G material is mesoporous composite. Also, the pore sized distribution curves calculated by BJH method shows a wide distribution at pore width of 3–60 nm, further confirming the presence of many mesopores (Fig. S3). The pore volume of the ultimate composite is 0.12 $cm^3\ g^{-1}$, which slightly lowers compared with the porous Si (0.37 $cm^3\ g^{-1}$), revealing the effective carbon coating and the formation of clusters after ball-milling [44]. The existence of mesopores can accommodate the volume expansion during the Li lithiation/delithiation process and raise the speed of the Li-ion transmission by shortening the diffusion pathways, which is beneficial for the cycling stability.

The morphology of the Al-Si alloy, the porous Si/G and the mesoporous Si@C/G composites are observed in the SEM as shown in Fig. 3. Smooth-faced Al-Si spheres with a size of around 20 μm can be seen in Fig. 3a. After the acid etching, the particle size decreases sharply, the surface becomes rough and apertured (Fig. 3b). The mesoporous Si@C/G composites are loose and porous with a uniform distribution of particle size as seen from Fig. 3c–e. And the particle size is in the range of dozens of nanometers to several micrometers, which ensures the integral uniformity of the material. Fig. 3f–h exhibits the mapping images of the Si, C and O elements. It's apparent that the Si element is wrapped in the carbon layer. The energy dispersive spectrometer (EDS) analysis is utilized to confirm the content of each element as shown in Table 1. We can see from Table 1 that the weight ratio of Si is 13.58%, which is much lower than the designed proportion (25%). This is probably owing to the coating effect of the amorphous carbon layer. In fact, there are many oxygen species in the fresh sample including adsorbed oxygen (such as H_2O, CO_2 and O_2), oxidized carbon, and SiO_2. As shown in Fig. S2 and Table S1, there is only a small amount of SiO_2 in the prepared sample. So, the main oxygen comes from the adsorbed oxygen and amorphous carbon. To further clarify content of the Si in the ultimate material, thermogravimetry (TG) analysis was conducted in the air. The TG-DTG-DSC curves are given in Fig. S4, revealing that the mass ratio of Si, G and C in the mesoporous Si@C/G is about 25:47:28, which is close to the designed ratio. The results from the SEM and the EDS are in accordance with the N_2 sorption

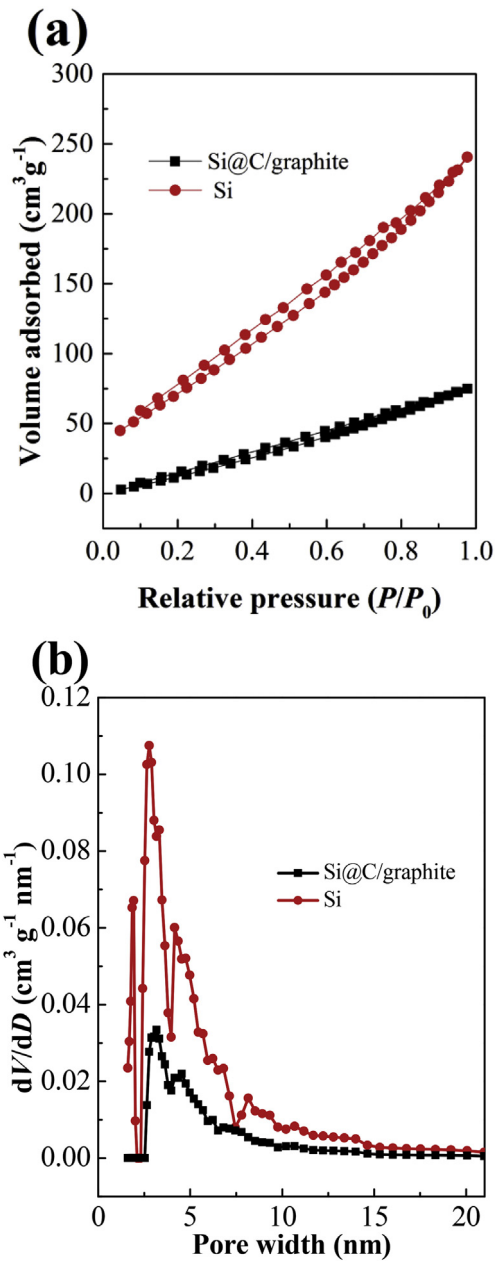

Fig. 2. N_2 adsorption isotherms (a) and the corresponding pore size distribution (b) of the porous Si and the porous Si@amorphous carbon/graphite (Si@C/G) composite.

isotherms and XRD patterns, confirming the existence of porous structure and the composition of the elemental.

The TEM and HRTEM images are given in Fig. 4, which are employed to elucidate the microstructure and the crystal lattice of the mesoporous Si@C/G materials. In Fig. 4a, the dark part is uniformly dispersing in the light section. To clarify the composition in the two parts, the selected area electron diffraction (SAED) analysis is applied and the results are shown in Fig. 4a inset. We can conclude that the crystal phase of the composite consists of silicon and graphite, which is in line with the XRD consequences. Fig. 4b shows the magnified images of the dark part in Fig. 4a. Clearly, there are many mesopores with width of 5 nm, which is in keeping with the pore size distribution consequences. This is probably caused by the Al digestion, forming many meso/macropores. Similar results were also reported on the Si-Al alloy-derived anode

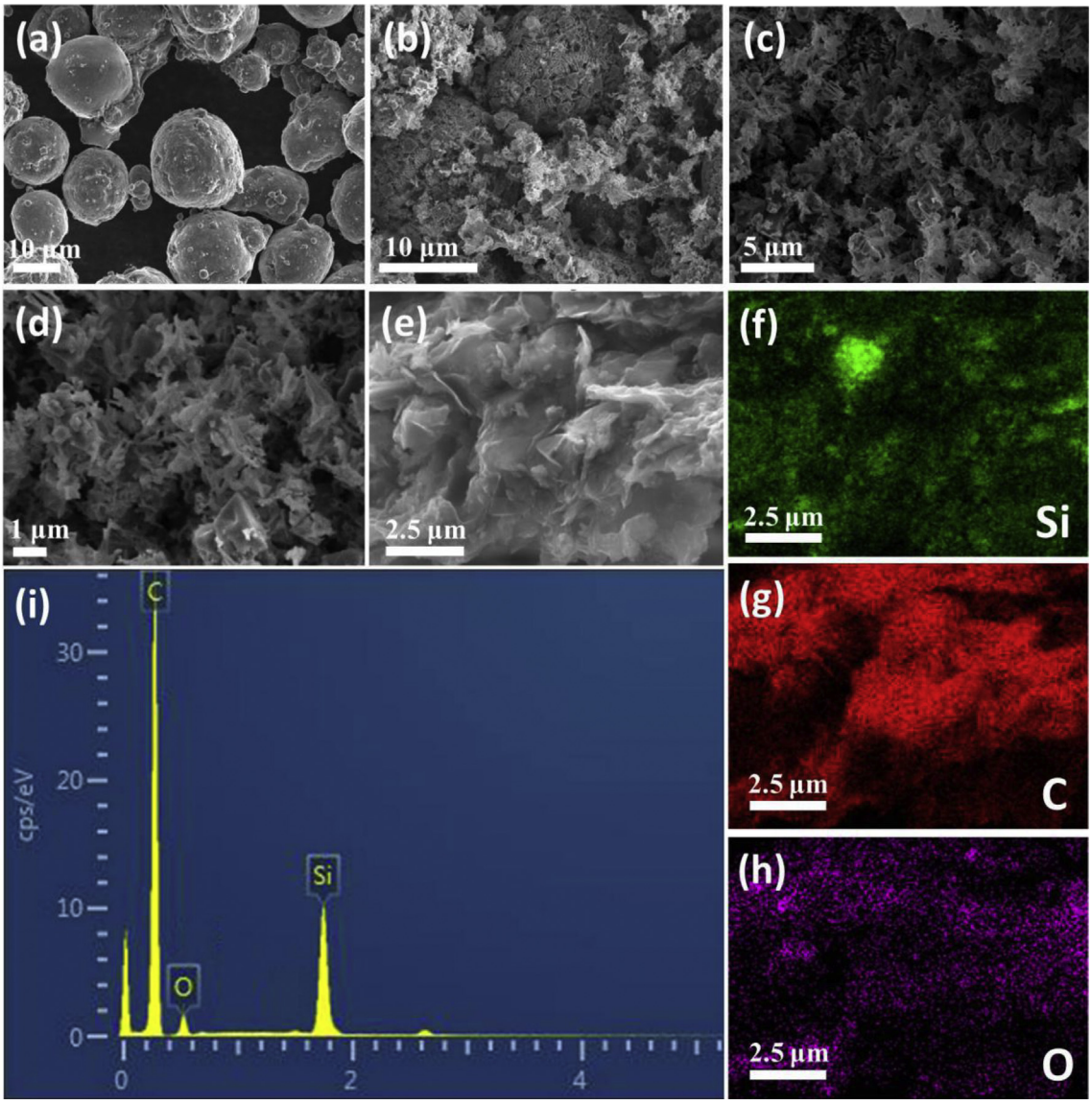

Fig. 3. SEM images of (a) Al-Si alloy, (b) porous Si/graphite and (c–e) mesoporous Si@amorphous carbon/graphite (Si@C/G) composite; Elemental mapping images of (f) Si, (g) C and (h) O in final products. EDS analysis (i) of as-prepared Si@C/G composite.

Table 1
Element analysis results derived from the EDS patterns in Fig. 3(i).

Element	Weight percent%	Atomic percent%
C	81.51	89.6
O	4.91	4.0
Si	13.58	6.4
Total	100.00	100.0

materials, where many nanopores were formed during the acid etching process [34,35]. Fig. 4c exhibits the magnified edge between the light part and the dark part in Fig. 4a. It can be observed that the particle is uniformly coated by a disordered carbon layer, ca.20 nm, which is in keeping with the EDS line result in Fig. 4e and f. The distinct lattice fringes in Fig. 4d with d-spacing of 0.31 nm can be readily indexed to the (111) plane of silicon. Broadly speaking, the structure of the as-prepared mesoporous Si@C/G composite is mesoporous Si particles wrapped in amorphous carbon layer and dispersed in graphite matrix, which is in coincidence with our design. The well contact of the silicon and the amorphous carbon layer can predictably buffer the large volumetric expansion of the Si when it reacts with Li, which is subservient for the structure integrity of the anode material [45,46]. The graphite acts as a support and matrix to enhance the conductive capacity of the material and avoid the collapse of the structure [47,48].

3.2. Electrochemical performance

The 1st, 2nd and 10th constant current charge and discharge profiles of the mesoporous Si@C/G anodes at 100 mA g^{-1} with a cutoff voltage ranging from 0.01 to 3 V versus Li^+/Li are presented in Fig. 5a. There is an unrepeatable plateau at about 0.75 V in the initial discharge profile in line with a dQ/dV peak of the initial discharge curve in Fig. 5b, which can be ascribed to the decomposition of electrolyte and the formation of solid electrolyte interface (SEI) layer. The consumption of Li^+ through this way results in the irreversible capacity of the first cycle [8,9,46]. When the battery discharges to 0.2–0.01 V, an obvious and long slant plateau

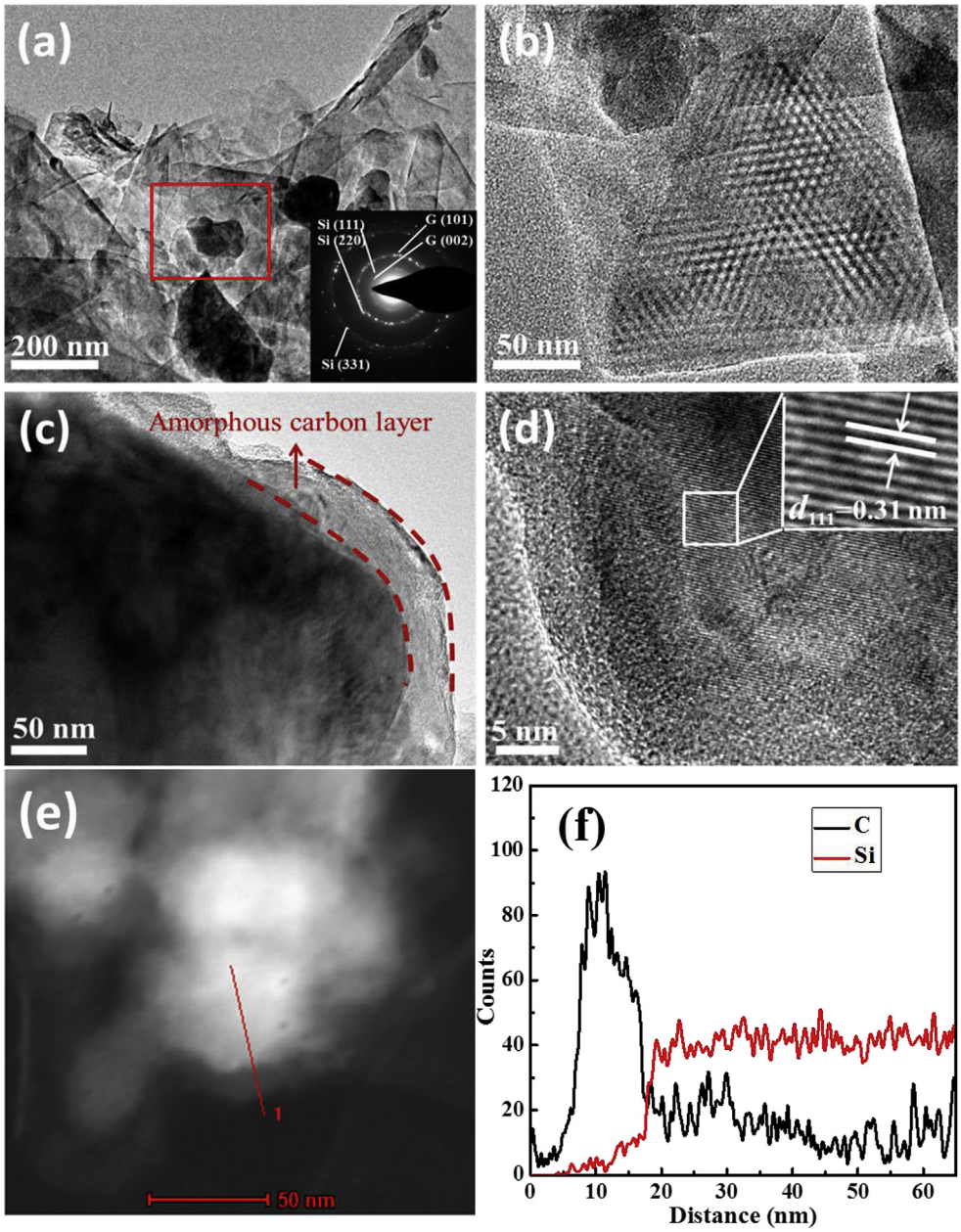

Fig. 4. TEM images of Si@C/G composite recorded at different magnifications: (a), (b), (c) TEM and (d) HRTEM; (e) and (f) EDS line result.

appears, which is caused by the lithiation reaction of the Si, the graphite and the amorphous carbon [49]. There is no obvious difference in discharge curves between 2nd and 10th cycle, reflecting a stable anode structure. The charge plateau at 0.1–0.2 V can be assigned to the delithiation of graphite, which concurs with the peaks located at 0.2 V in Fig. 5b. The delithiation reaction of silicon occurs at about 0.5 V, which is presented as a long plateau in Fig. 5a. The charge profiles of 1st, 2nd, 10th have only slight difference, indicating an excellent reversibility of the anodes.

To further investigate the reversibility of the anodes, the cyclic voltammogram (CV) is applied. Fig. 6 shows the CV profiles of the mesoporous Si@C/G anode along with a scanning potential of 0–3.0 V (vs. Li^+/Li) at a scanning speed of 0.1 mV s^{-1}. Three cathodic current peaks appear at 0.75, 0.10 and 0.01 V in the initial scanning loop, which is attributed to the reaction between Li and the electrolyte, graphite as well as Si, respectively. Furthermore, three anodic peaks located at 0.12, 0.35, 0.50 V are observed obviously. The peak at 0.12 V corresponds to the delithiation of graphite, and the peaks at 0.33 V and 0.5 V are attributed to a two-step process of lithium extraction from Li_xSi to Si [2,50,51]. The results in the CV profiles are in well accordance with the plateaus and the peaks observed in Fig. 5a and b. The peak current values increase along with discharge-charge cycles corresponding to the activation of materials, whereas the peak location is basically in coincidence with the first cycle, indicating there are no other reactions occurring during the subsequent cycles. Fig. 6b shows the CV profiles of 6–10 cycles with a same scanning rate. The increases of the peak current are not as much as that during 1–5 cycles, indicating that the material comes to a steady state after 10 cycles. The location of the current peaks ranges a little of about 0.05 V during the anodic and cathodic scanning, reflecting an excellent reversibility of the reaction between Li^+ and active material. The CV profiles at

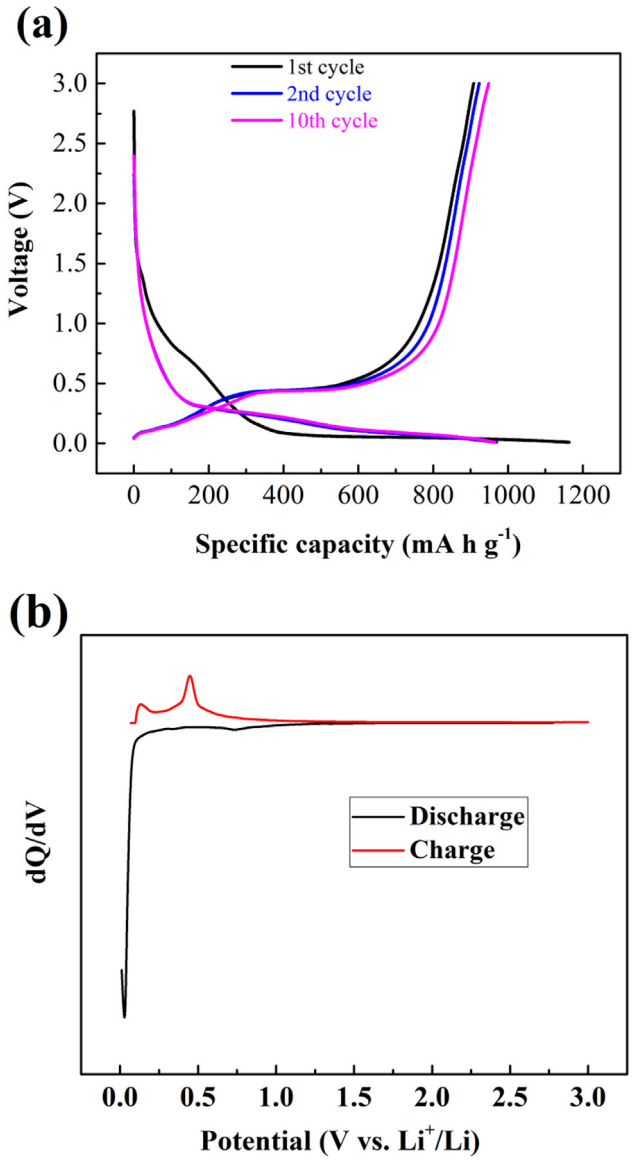

Fig. 5. (a) Galvanostatic charge-discharge voltage profiles for different cycles, (b) dQ/dV curves for the initial charge and discharge profile.

different scanning rates ranging between 0.1 and 0.5 mV s^{-1} are investigated and exhibited in Fig. 6c. Along with the increasing of the scanning rate, the electrochemical polarization and the increase of the current peaks become more and more dramatic. The location of the anodic peaks shifts positively and the cathodic peaks shift negatively, suggesting a decreasing reversibility of the material.

A comparison between the mesoporous Si@C/G and the pristine Si@C/G materials is made to demonstrate the advantage of the porous nature of the Si on its electrochemical property. The initial discharge and charge specific capacities of the latter are 1267.0 and 985.6 mAh g^{-1}, respectively, with the ICE of 77.8% (Fig. 7a). After 50 cycles, about 75% of the reversible specific capacity is retained. The mesoporous Si@C anode holds a reversible specific capacity of 860 mAh g^{-1} after 50 cycles and the reversible specific capacity maintains 95%. The mesoporous Si@C/G anode holds high initial discharge capacity of 1158.0 mAh g^{-1}, which is in accordance with the calculated value (25%*3700 + 47%*372 + 28% *520 = 1240 mAh g^{-1}). Its ICE is 78.4%, much higher than that of the mesoporous Si@C and the previous reports [35]. The coulombic

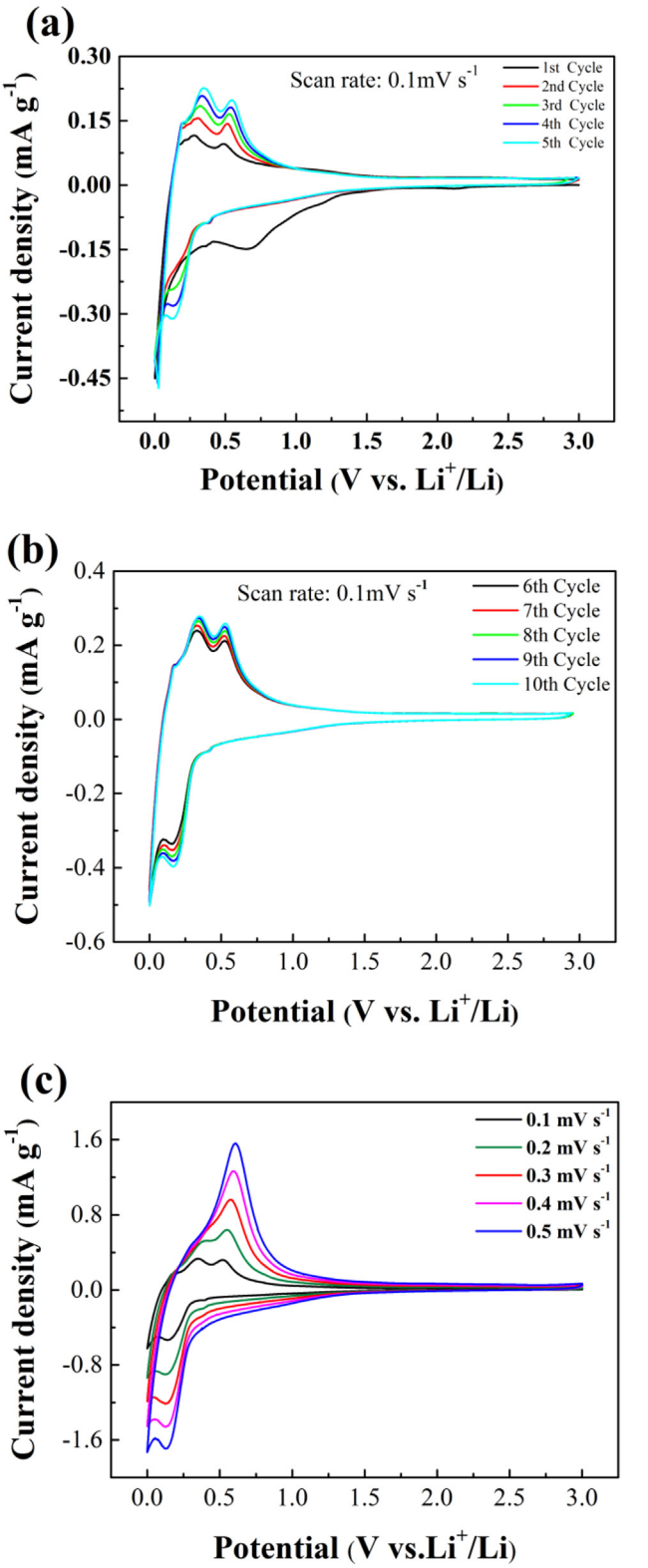

Fig. 6. Cyclic voltammogram profiles (a) during 1–5 cycles, (b) during 6–10 cycles, (c) at different scan rates.

efficiency (CE) reaches 98% soon after 5 cycles and the retained capacity still keeps 919.0 mAh g^{-1} after 150 cycles, about 79.36% of the initial discharge capacity, suggesting that the mesoporous Si@C/G electrodes have excellent cycle stability and

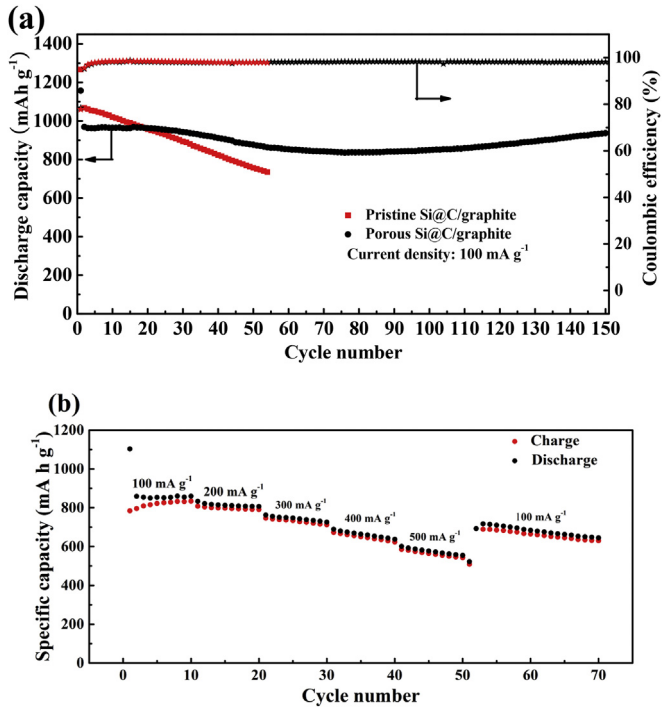

Fig. 7. Cycle performance of the Si@amorphous carbon/graphite (Si@C/G) and the prinstine Si@C/G electrodes (a) at 100 mA g^{-1} and the rate performance of the mesoporous Si@C/G electrode (b).

electrochemical performance. It is notable that the initial discharge capacity of the mesoporous Si@C/graphite is a little lower than that of the pristine Si@C/graphite, probably duo to the formation of a number of SiO_2 during the HCl etching process (Fig. S2). Table S2 lists a number of Si-based anodes. Clearly, the mesoporous Si@C/G electrode exhibits comparable electrochemical performance to most of the Si-based anodes, indicating a promising anode material. The modified cycling stability is mainly due to the special pore structure and the introduction of the graphite as seen in Figs. 3 and 4. Firstly, the existence of the mesopores in the ultimate material can serve as a kind of buffer matrix during the lithiation/delithiation process and enhance the speed of the Li-ion transmission. Secondly, the homogeneous mixing of porous Si, graphite and amorphous carbon observed from the SEM images (Fig. 3) can preserve the integrality of the electrodes during cycling. What's more, the outside carbon layer revealed from the HRTEM images (Fig. 4), the elemental mapping images and the EDS results (Fig. 3) isolate the immediate contact between the Si and electrolyte, forming a stable SEI and emerging an excellent reversibility of the electrodes. Eventually, the addition of graphite can boost the electric contact and reduce the polarization resistance.

The cycling stability of Si/graphite, Si/C and pure mesoporous Si are shown in Fig. S5. From this figure, it can be observed that the pure mesoporous Si shows low cycle stability. After 20 cycles, the capacity of pure mesoporous Si decrease to ~12 mAh g^{-1}. After mixing with graphite and amorphous carbon, its cycle stability increases sharply. Noticeably, the stability and capacity of the Si@C/G are much higher than those of Si/G and Si/C. Because the mesoporous structure of Si and outer carbon layer can refrain the volume expansion of composite material during the lithium insertion/extraction process and create efficient channels for the fast transport of Li^+. Furthermore, the graphite can efficiently improve the electroconductibility of the anode material. So, a suitable ratio of Si, C and graphite can complement each other's advantages, increasing its electrochemical performance. The SEM images of the mesoporous Si@C/G electrode before and after 150 cycles are shown in Fig. S6. Noticeably, only several cracks can be observed on the surface of the composite. And a relatively smooth structure has also been kept after 150 cycles, indicating good stability of the anode material.

Fig. 7b shows the rate performance of the mesoporous Si@C/G electrode at different current densities varying between 100 and 500 mA g^{-1}. The current density of the first 10 cycles is 100 mA g^{-1}, raising 100 mA g^{-1} every 10 cycles and finally restoring to 100 mA g^{-1}. The capacity of the above electrode decreases following the increasing current densities. When the current density maximizes to 500 mA g^{-1}, a reversible capacity of the anode can maintain about 550 mAh g^{-1}. When it returns to 100 mA g^{-1}, its capacity drops from ~720 to ~645 mAh g^{-1}. This is caused by the volumetric expansion of mesoporous Si. At small current density, the lithium ions would gradually insert into the Si nanoparticles. And more active material would be utilized. So the mesoporous Si@C/G electrode exhibits high cycle stability. However, the electrode polarization and irreversibility of the material increase with elevated the current density. After coating with carbon, these phenomena would be alleviated but cannot be eliminated. And high current density would still result in electrode polarization and irreversibility of the mesoporous Si. This is in good accordance with the cyclic voltammogram profiles at different scan rates (Fig. 6c). From Fig. 7 and Fig. S5, we can see that the electrochemical performance of mesoporous Si@C/graphite improves obviously as compared with those of Si/G, Si/C and pure mesoporous Si. The prominent rate performance can be assumed to the outstanding electronic conductivity of the graphite and the integrality of the structure during lithiation and delithiation.

To further clarify the reasons for the improved electrochemical performance, the EIS analysis is applied for the mesoporous Si@C/G composite at different cycles. The Nyquist diagrams of the ultimate composite electrode for the fresh, 1st, 2nd and 50th cycles are presented in Fig. 8a. All the impedance spectra are constitutive of a semicircle in high frequency and a following slash in low frequency, which is assigned to the interface electrochemical polarization resistance (Rp) and the Warburg impedance (Zw), respectively [50,52]. The impedance data agree well with the proposed equivalent circuit (Fig. 8a inset), which includes the solution resistance (Rs), the interface electrochemical polarization resistance (Rp), the constant phase element (CPE) between the interface of the electrode and the electrolyte, and the Warburg impedance (Zw) [50].

From Fig. 8a, the Rp of the fresh state is 140.2 Ω, whereas it decreases to 89.2 Ω when firstly discharging to 0.01 V. After 50 cycles, it increases to 125.2 Ω due to the slightly oxidation process of the anode material in the electrolyte during cycling [53]. This result shows that the Rp changes slightly with the adding of the cycle number. It implies that the chemical/mechanical film on the active material/electrolyte interface is stable during cycles, which leads to an excellent electrochemical performance [50]. Furthermore, a comparison between the pristine Si@C/G and the porous Si@C/G is exhibited in Fig. 8b with the resistance values of 133.3 and 88.7 Ω when firstly discharging to 0.01 V, respectively. The reduction of the resistance can be attributed to the increasing of the electric conductivity caused by the porous structure of the composite material. The uniform carbon layer outside the silicon hinders the collapse of the structure, which is beneficial to the cycling performance.

4. Conclusions

We demonstrate an eco-friendly and low-cost approach to synthesize a mesoporous Si@C/G composite through an acid

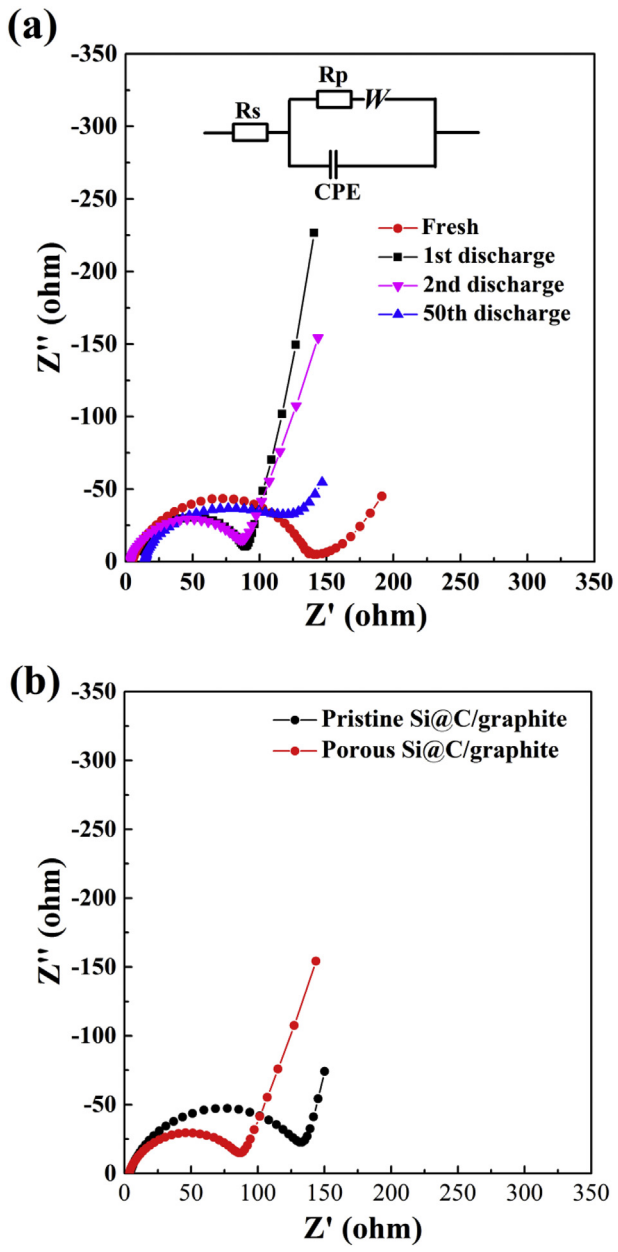

Fig. 8. Nyquist plots of the Si@ amorphous carbon/graphite (Si@C/G) composite at different cycles (a) and comparison of the pristine Si@C/G and the porous Si@C/G electrodes (b).

etching on a low-cost Al-Si alloy followed by the ball-milling and heat treatment process. The as-prepared composite delivers an initial lithiation capacity of 1158.0 mAh g^{-1} with an ICE of 78.4%, along with a reversible capacity of 919.0 mAh g^{-1} after 150 cycles. Compared with other porous Si/C materials and the pristine Si@C/G, the composite shows a much higher residual capacity and initial coulombic efficiency. The introduction of the mesopores and the uniform carbon layer outside the Si can buffer the volume expansion during the forming process of Li-Si alloy phase, and the addition of graphite can improve the electronic conductibility. Furthermore, owing to this eco-friendly synthesis process, the low-cost raw material, and the stable electrochemical performance in this work, the mesoporous Si@C/G electrodes are potential to achieve the industrial applications in commercialized LIBs.

Acknowledgements

This work was supported by the Program of China (2011AA11A255), Natural Science Foundation of Tianjin, China (13JCZDJC32000) and the MOE Innovation Team (IRT13022).

Appendix A. Supplementary data

Supplementary data related to this article can be found at http://dx.doi.org/10.1016/j.jallcom.2017.08.244.

References

[1] J.L. Gómez-Cámer, H. Thuv, P. Novák, Electrochemical study of Si/C composites with particulate and fibrous morphology as negative electrodes for lithium-ion batteries, J. Power Sources 294 (2015) 128–135.
[2] W. Wu, Y. Liang, H. Ma, Y. Peng, H. Yang, Insights into the conversion behavior of SiO-C hybrid with pre-treated graphite as anodes for Li-ion batteries, Electrochim. Acta 187 (2016) 473–479.
[3] Y.S. Hu, R. Demir-Cakan, M.M. Titirici, J.O. Muller, R. Schlogl, M. Antonietti, J. Maier, Superior storage performance of a Si@SiO_x/C nanocomposite as anode material for lithium-ion batteries, Angew. Chem. Int. Ed. 47 (2008) 1645–1649.
[4] B. Liang, Y. Liu, Y. Xu, Silicon-based materials as high capacity anodes for next generation lithium ion batteries, J. Power Sources 267 (2014) 469–490.
[5] M.S. Wang, W.L. Song, J. Wang, L.Z. Fan, Highly uniform silicon nanoparticle/porous carbon nanofiber hybrids towards free-standing high-performance anodes for lithium-ion batteries, Carbon 82 (2015) 337–345.
[6] Z. Li, W. Wang, Z. Li, Z. Qin, J. Wang, Z. Liu, Bridging porous Si–C composites with conducting agents for improving battery cycle life, J. Power Sources 286 (2015) 534–539.
[7] M. Sohn, D.S. Kim, H.I. Park, J.H. Kim, H. Kim, Porous silicon–carbon composite materials engineered by simultaneous alkaline etching for high-capacity lithium storage anodes, Electrochim. Acta 196 (2016) 197–205.
[8] J. Zhang, Y. Liang, Q. Zhou, Y. Peng, H. Yang, Enhancing electrochemical properties of silicon-graphite anodes by the introduction of cobalt for lithium-ion batteries, J. Power Sources 290 (2015) 71–79.
[9] J. Shi, Y. Liang, L. Li, Y. Peng, H. Yang, Evaluation of the electrochemical characteristics of silicon/lithium titanate composite as anode material for lithium ion batteries, Electrochim. Acta 155 (2015) 125–131.
[10] L. Hu, H. Wu, S.S. Hong, L. Cui, J.R. McDonough, S. Bohy, Y. Cui, Si nanoparticle-decorated Si nanowire networks for Li-ion battery anodes, Chem. Commun. 47 (2011) 367–369.
[11] Y. Zhou, X. Jiang, L. Chen, J. Yue, H. Xu, J. Yang, Y. Qian, Novel mesoporous silicon nanorod as an anode material for lithium ion batteries, Electrochim. Acta 127 (2014) 252–258.
[12] H. Wu, Y. Cui, Designing nanostructured Si anodes for high energy lithium ion batteries, Nano Today 7 (2012) 414–429.
[13] J.P. Maranchi, A.F. Hepp, P.N. Kumta, High Capacity, Reversible silicon thin-film anodes for lithium-ion batteries, Electrochem. Solid-State Lett. 6 (2003) A198.
[14] J.Z. Wang, C. Zhong, S.L. Chou, H.K. Liu, Flexible free-standing graphene-silicon composite film for lithium-ion batteries, Electrochem. Commun. 12 (2010) 1467–1470.
[15] T. Yamada, H. Itahara, H. Yamane, Preparation of micro-porous Si particles from Mg_2Si powder, Mater. Lett. 98 (2013) 157–160.
[16] H. Jia, P. Gao, J. Yang, J. Wang, Y. Nuli, Z. Yang, Novel three-dimensional mesoporous silicon for high power lithium-ion battery anode material, Adv. Energy Mater. 1 (2011) 1036–1039.
[17] J.H. Byeon, Y.-W. Kim, Ambient plasma synthesis of Si-Fe hollow nanoparticles and their biocompatibility and lithium storage capacity, Adv. Mater. Interfaces 1 (2014) 1300134.
[18] G.X. Wang, J.H. Ahn, J. Yao, S. Bewlay, H.K. Liu, Nanostructured Si–C composite anodes for lithium-ion batteries, Electrochem. Commun. 6 (2004) 689–692.
[19] M. Yoshio, H.Y. Wang, K. Fukuda, T. Umeno, N. Dimov, Z. Ogumi, Carbon-coated Si as a lithium-ion battery anode material, J. Electrochem. Soc. 149 (2002) A1598–A1603.
[20] R. Zhou, R. Fan, Z. Tian, Y. Zhou, H. Guo, L. Kou, D. Zhang, Preparation and characterization of core–shell structure Si/C composite with multiple carbon phases as anode materials for lithium ion batteries, J. Alloys Compd. 658 (2016) 91–97.
[21] J. Chen, X. Lu, J. Sun, F. Xu, Si@C nanosponges application for lithium ions batteries synthesized by templated magnesiothermic route, Mater. Lett. 152 (2015) 256–259.
[22] J.B. Park, K.H. Lee, Y.J. Jeon, S.H. Lim, S.M. Lee, Si/C composite lithium-ion battery anodes synthesized using silicon nanoparticles from porous silicon, Electrochim. Acta 133 (2014) 73–81.
[23] M.K. Datta, J. Maranchi, S.J. Chung, R. Epur, K. Kadakia, P. Jampani, P.N. Kumta, Amorphous silicon–carbon based nano-scale thin film anode materials for lithium ion batteries, Electrochim. Acta 56 (2011) 4717–4723.
[24] Z. Zhang, Y. Wang, W. Ren, Q. Tan, Y. Chen, H. Li, Z. Zhong, F. Su, Scalable

synthesis of interconnected porous silicon/carbon composites by the Rochow reaction as high-performance anodes of lithium ion batteries, Angew. Chem. Int. Ed. 53 (2014) 5165–5169.
[25] X. Zhao, C.M. Hayner, M.C. Kung, H.H. Kung, In-plane vacancy-enabled high-power Si-graphene composite electrode for lithium-ion batteries, Adv. Energy Mater. 1 (2011) 1079–1084.
[26] I. Hong, B. Scrosati, F. Croce, Mesoporous, Si/C composite anode for Li battery obtained by 'magnesium-thermal' reduction process, Solid State Ionics 232 (2013) 24–28.
[27] X. Ma, M. Liu, L. Gan, P.K. Tripathi, Y. Zhao, D. Zhu, Z. Xu, L. Chen, Novel mesoporous Si@C microspheres as anodes for lithium-ion batteries, Phys. Chem. Chem. Phys. 16 (2014) 4135–4142.
[28] R. Zhang, Y. Du, D. Li, D. Shen, J. Yang, Z. Guo, H.K. Liu, A.A. Elzatahry, D. Zhao, Highly reversible and large lithium storage in mesoporous Si/C nano-composite anodes with silicon nanoparticles embedded in a carbon frame-work, Adv. Mater. 26 (2014) 6749–6755.
[29] N. Liu, H. Wu, M.T. McDowell, Y. Yao, C. Wang, Y. Cui, A yolk-shell design for stabilized and scalable li-ion battery alloy anodes, Nano Lett. 12 (2012) 3315–3321.
[30] L. Su, J. Xie, Y. Xu, L. Wang, Y. Wang, M. Ren, Preparation and lithium storage performance of yolk-shell Si@void@C nanocomposites, Phys. Chem. Chem. Phys. 17 (2015) 17562–17565.
[31] A. Magasinski, P. Dixon, B. Hertzberg, A. Kvit, J. Ayala, G. Yushin, High-performance lithium-ion anodes using a hierarchical bottom-up approach, Nat. Mater. 9 (2010) 353–358.
[32] J. Deng, H. Ji, C. Yan, J. Zhang, W. Si, S. Baunack, S. Oswald, Y. Mei, O.G. Schmidt, Naturally rolled-up C/Si/C trilayer nanomembranes as stable anodes for lithium-ion batteries with remarkable cycling performance, Angew. Chem. Int. Ed. 52 (2013) 2326–2330.
[33] M. Ge, Y. Lu, P. Ercius, J. Rong, X. Fang, M. Mecklenburg, C. Zhou, Large-scale fabrication, 3D tomography, and lithium-ion battery application of porous silicon, Nano Lett. 14 (2014) 261–268.
[34] Z. Jiang, C. Li, S. Hao, K. Zhu, P. Zhang, An easy way for preparing high performance porous silicon powder by acid etching Al–Si alloy powder for lithium ion battery, Electrochim. Acta 115 (2014) 393–398.
[35] H. Tian, X. Tan, F. Xin, C. Wang, W. Han, Micro-sized nano-porous Si/C anodes for lithium ion batteries, Nano Energy 11 (2015) 490–499.
[36] H. Jiang, X. Zhou, G. Liu, Y. Zhou, H. Ye, Y. Liu, K. Han, Free-standing Si/graphene paper using Si nanoparticles synthesized by acid-etching Al-Si alloy powder for high-stability Li-ion battery anodes, Electrochim. Acta 188 (2016) 777–784.
[37] X. Ma, Y.L. Liu, L.L. Kong, Y.H. Ding, J. Zhao, N. Xu, Lithium-ion battery anode electrochemical properties of Si/C composites using graphite and glucose as carbon source, in: W. Pan, J.X. Ren, Y.G. Li (Eds.), Renewable and Sustainable Energy, Pts 1–7, Trans Tech Publications Ltd, Stafa-Zurich, 2012, pp. 3506–3509.
[38] Z.Y. Wang, Y. Li, J.Y. Lee, Characterizations of Al–Y thin film composite anode materials for lithium-ion batteries, Electrochem. Commun. 11 (2009) 1179–1182.
[39] J. Saint, M. Morcrette, D. Larcher, L. Laffont, S. Beattie, J.P. Pérès, D. Talaga, M. Couzi, J.M. Tarascon, Towards a fundamental understanding of the improved electrochemical performance of silicon–carbon composites, Adv. Funct. Mater. 17 (2007) 1765–1774.
[40] Y. Xu, G. Yin, Y. Ma, P. Zuo, X. Cheng, Nanosized core/shell silicon@carbon anode material for lithium ion batteries with polyvinylidene fluoride as carbon source, J. Mater. Chem. 20 (2010) 3216.
[41] Z.P. Guo, E. Milin, J.Z. Wang, J. Chen, H.K. Liu, Silicon/disordered carbon nanocomposites for lithium-ion battery anodes, J. Electrochem. Soc. 152 (2005) A2211.
[42] M. Kruk, M. Jaroniec, Gas adsorption characterization of ordered organic-inorganic nanocomposite materials, Chem. Mater. 13 (2001) 3169–3183.
[43] Y.P. Zhu, Y.P. Liu, T.Z. Ren, Z.Y. Yuan, Self-supported cobalt phosphide mesoporous nanorod arrays: a flexible and bifunctional electrode for highly active electrocatalytic water reduction and oxidation, Adv. Funct. Mater. 25 (2015) 7337–7347.
[44] J. Wu, Z. Zhu, H. Zhang, H. Fu, H. Li, A. Wang, H. Zhang, Z. Hu, A novel nano-structured interpenetrating phase composite of silicon/graphite–tin for lithium-ion rechargeable batteries anode materials, J. Alloys Compd. 596 (2014) 86–91.
[45] H.C. Tao, M. Huang, L.Z. Fan, X. Qu, Interweaved Si@SiOx/C nanoporous spheres as anode materials for Li-ion batteries, Solid State Ionics 220 (2012) 1–6.
[46] W. Wu, J. Shi, Y. Liang, F. Liu, Y. Peng, H. Yang, A low-cost and advanced SiOx-C composite with hierarchical structure as an anode material for lithium-ion batteries, Phys. Chem. Chem. Phys. 17 (2015) 13451–13456.
[47] S. Flandrois, B. Simon, Carbon materials for lithium-ion rechargeable batteries, Carbon 37 (1999) 165–180.
[48] H. Kim, M. Seo, M.H. Park, J. Cho, A critical size of silicon nano-anodes for lithium rechargeable batteries, Angew. Chem. Int. Ed. 49 (2010) 2146–2149.
[49] M.S. Wang, L.Z. Fan, M. Huang, J. Li, X. Qu, Conversion of diatomite to porous Si/C composites as promising anode materials for lithium-ion batteries, J. Power Sources 219 (2012) 29–35.
[50] X. Chen, X. Li, F. Ding, W. Xu, J. Xiao, Y. Cao, P. Meduri, J. Liu, G.L. Graff, J.G. Zhang, Conductive rigid skeleton supported silicon as high-performance Li-ion battery anodesm, Nano Lett. 12 (2012) 4124–4130.
[51] J. Xie, G. Wang, Y. Huo, S. Zhang, G. Cao, X. Zhao, Nanostructured silicon spheres prepared by a controllable magnesiothermic reduction as anode for lithium ion batteries, Electrochim. Acta 135 (2014) 94–100.
[52] Y. Liu, Z.Y. Wen, X.Y. Wang, A. Hirano, N. Imanishi, Y. Takeda, Electrochemical behaviors of Si/C composite synthesized from F-containing precursors, J. Power Sources 189 (2009) 733–737.
[53] H. Wu, G. Chan, J.W. Choi, I. Ryu, Y. Yao, M.T. McDowell, S.W. Lee, A. Jackson, Y. Yang, L. Hu, Y. Cui, Stable cycling of double-walled silicon nanotube battery anodes through solid-electrolyte interphase control, Nat. Nanotechnol. 7 (2012) 310–315.